COMMUNICATION

ChemComm
www.rsc.org/chemcomm

Atomic force microscopy study of the molecular sieve MnAPO-50

L. Itzel Meza,[a] Jonathan R. Agger,*[a] Nataša Z. Logar,[b] Venčeslav Kaučič[b] and Michael W. Anderson[a]

[a] *UMIST Centre for Microporous Materials, Department of Chemistry, UMIST, PO Box 88, Manchester, UK M60 1QD. E-mail: j.agger@umist.ac.uk; Fax: +44 161 200 4559; Tel: +44 161 200 4527*

[b] *National Institute of Chemistry, Hajdrihova 19, 1000 Ljubljana, Slovenia*

Received (in Cambridge, UK) 9th May 2003, Accepted 25th July 2003
First published as an Advance Article on the web 6th August 2003

Atomic force microscopy (AFM) imaging of MnAPO-50 reveals multiply-nucleated, elliptical terraces, oriented in registry with the facet edges with step heights ranging from one to six template repeat distances on the {100} facets and terraces with step heights ranging from one to thirty three times the *c* unit cell parameter on the {001} facets.

Aluminophosphate molecular sieves have uncharged frameworks and thus no cations which could act as Brønsted acid sites for catalysis. Charge can be introduced by incorporating heteroatoms into the framework, with the creation of Brønsted, Lewis and redox-acid sites, and it is of interest to examine the morphological consequences of such incorporation to further our limited understanding of crystallisation processes in open framework materials generally.

Of the currently available techniques: high-resolution transmission electron microscopy (HRTEM) provides detailed imaging of surfaces in cross-section, highlighting terminations and terrace steps;[1] scanning electron microscopy (SEM) permits observation of nanometre-scale surface features on multiple crystals simultaneously,[2,3] affording excellent global surface characterisation, however terrace height information is not easily obtained; atomic force microscopy (AFM), invented in 1986 by Binning *et al.*,[4] permits quantitative atomic-scale surface imaging of insulating samples.

AFM was first used to study cleaved surfaces of natural zeolites such as clinoptilolite,[5] heulandite,[6,7] mordenite,[8] stilbite[7] and this research led to the surface investigation of synthetic zeolites such as zeolite X,[2] zeolite Y,[9,10] mordenite,[11,12] zeolite A,[2,3,10,12–15] and silicalite.[2,10,16] Recently, zincophosphate crystals were imaged using AFM as part of a study into reverse micelle synthetic methods.[17]

In this study we have used atomic force microscopy to image the surface of MnAPO-50. This work constitutes only the second ever AFM study of a metal-substituted aluminophosphate material. MnAPO-50 is of particular interest since it has never been crystallised as pure aluminophosphate – metal incorporation appears prerequisite. Improving our understanding of the crystallisation of this material might ultimately afford an explanation for this phenomenon. Moreover, control of [001] growth for crystals with a unidimensional pore system has important ramifications for catalytic performance as it governs access to the internal surface. Whilst this material has a three dimensional pore system, the larger 12-ring pores run only along [001].

Crystallisation was carried out hydrothermally from a gel with the following composition:

$$0.3\ MnO : 0.75\ Al_2O_3 : 1\ P_2O_5 : 4\ Pr_2NH : 50\ H_2O$$

The synthesis was conducted in the presence of di-*n*-propylamine and manganese(II) acetate – exact details are reported elsewhere.[18] The crystals have hexagonal prismatic morphology with dimensions from $50 \times 50 \times 100$ to $100 \times 100 \times 300\ \mu m^3$, Fig. 1(a), and some intergrowth is observed, Fig. 1(b). Single crystal X-ray diffraction reveals the MnAPO-50 framework possesses 12-ring channels running along [001], as shown in Fig. 1(c), connected to an 8-ring channel system running along $<100>$, as shown in Fig. 1(d). The hexagonal unit cell parameters are: $a = 12.746$ Å and $c = 9.140$ Å.[18] The chemical composition of crystals used in this study is:

$$(Mn_{0.46}\ Al_{0.54})\ PO_4 : 0.33\ Pr_2NH : 0.125\ H_2O.$$

Protonated template and the existence of some trivalent manganese preserves charge neutrality. AFM images were recorded on a NanoScope III operating in TappingMode™ as detailed elsewhere.[13]

Micrographs of {100} faces show that MnAPO-50 grows *via* the deposition of successive layers similar to that observed for zeolites A,[3,13] Y,[9] X and L,[2] silicalite[16] and ZnPO-X.[17] The {100} face exhibits elliptical terraces growing outwards from multiple nucleation points, one of which is shown in Fig. 2(a). Prior to coalescence the elliptical eccentricity of the terraces appears constant at 0.91 ± 0.01 and the principle axes are aligned in registry with one another and the facet edges – the major axis along [001] and the minor axis along $<100>$. This implies that growth rates in the [001] and $<100>$ directions must each be constant. Terrace behaviour upon coalescence, as shown in Fig. 2(b), is intermediate between that observed for zeolite A[13] and for SSZ-42,[19] as exemplified in Fig. 2(c) and 2(d) respectively. Terrace coalescence on {100} faces of zeolite A results in rapid KINK site growth with the initial formation of curved terrace edges quickly leading to blocking out. Modelling of zeolite A suggests growth at KINK sites is 15 times more likely than growth at EDGE sites.[15] A schematic of EDGE and KINK sites is shown in Fig. 2(e). Terrace coalescence on {110}

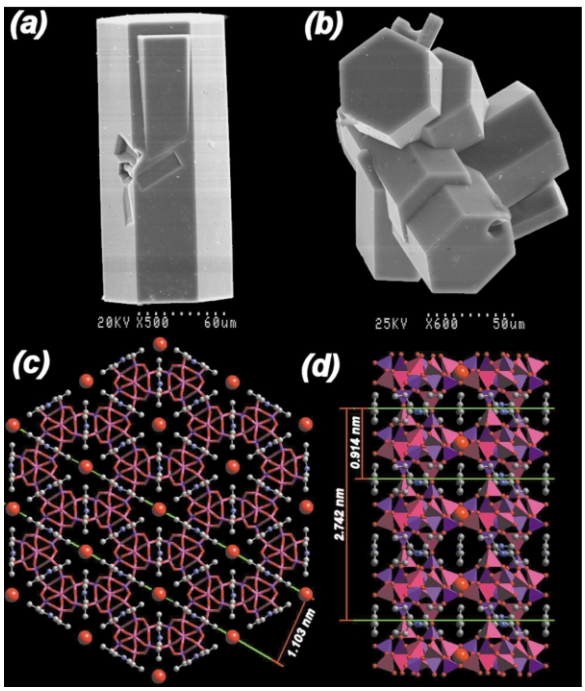

Fig. 1 (a) and (b) SEM images of MnAPO-50 crystals. (c) MnAPO-50 framework showing 12-ring channels running along [001]. (d) 8-ring channel system running along $<100>$ with single and triple multiples of the *c* unit cell parameter highlighted. Pore water is located by the oxygen atoms shown.

DOI: 10.1039/b305253b

faces of SSZ-42 implies a degree of parity between growth at KINK sites and EDGE sites, evidenced by the persistence of the cusp shaped coalescence points. Towards the edge of the MnAPO-50 crystal the elliptical terraces become more angular, as shown in Fig. 2(f). This implies an increase in the likelihood of growth at KINK sites, which are responsible for the blocking out phenomenon. This further implies a decrease in the attachment energy at such sites. Two explanations are possible: manganese zoning; changes in gel composition during growth. Cross-sectional analysis reveals terrace heights are multiples of 1.1 nm, as shown in Fig. 2(g), up to a maximum of six. This multiple corresponds well to the < 100 > template *d*-spacing of 1.103 nm, as shown in Fig. 1(c). Terrace height measurement has an associated error of ± 0.2 nm. Dissolution pits as deep as *ca.* 39 nm are observed on the {100} face as shown in Fig. 2(h).

Fig. 3(a) shows the surface topography of a hexagonal (001) face of an MnAPO-50 crystal. The surface exhibits layers with saw-tooth edges, shown at greater magnification in Fig. 3(b). Analysis of the layers, Fig. 3(c), reveals step heights in multiples of 0.9 nm, corresponding to the *c* unit cell parameter of 0.914 nm, as shown in Fig. 1(d). Terraces of up to 33 multiples were found.

In tandem with other microporous materials, MnAPO-50 appears to grow *via* layer upon layer deposition. Multiple terrace nucleation is evident on {100} facets. Both {100} and (001) facets exhibit multiple layer stacking with the phenomenon being more pronounced on the latter. This has been observed for silicalite and has been attributed to defect formation. Work is underway to better understand the occurrence of this phenomenon in the MnAPO-50 structure.

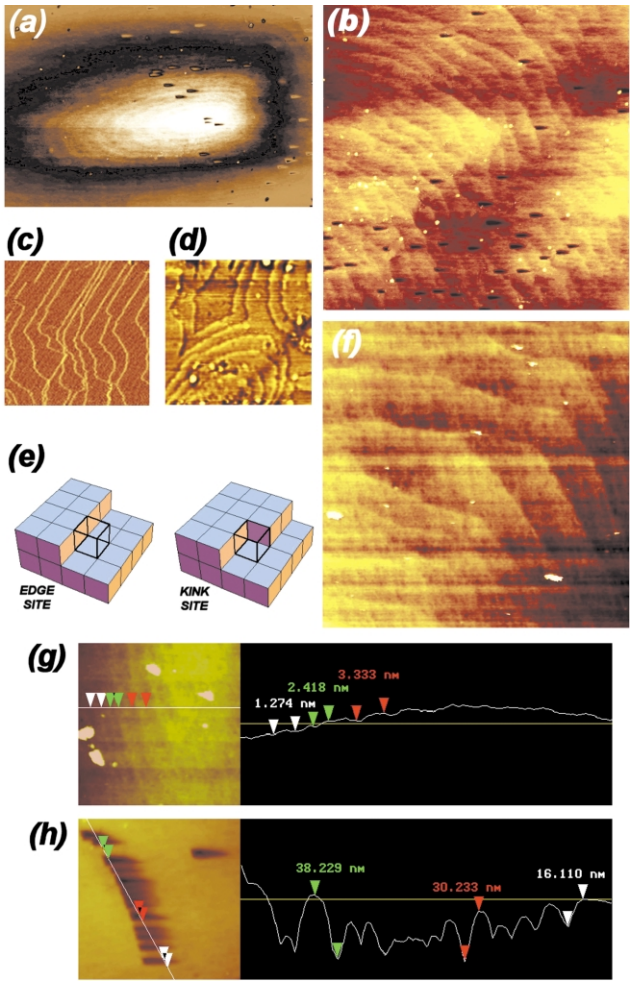

Fig. 2 (a) 8.8 × 5.3 μm² and (b) 6.3 × 6.3 μm² height images of MnAPO-50 {100} faces. (c) and (d) show terrace coalescence behaviour of zeolite A and SSZ-42 respectively. (e) wire frame depictions of EDGE and KINK sites. (f) 5.8 × 5.8 μm² height image of terraces approaching the {100} facet edge of MnAPO-50. (g) cross-sectional analysis of terraces on {100} faces. (h) section analysis of dissolution pits on {100} faces.

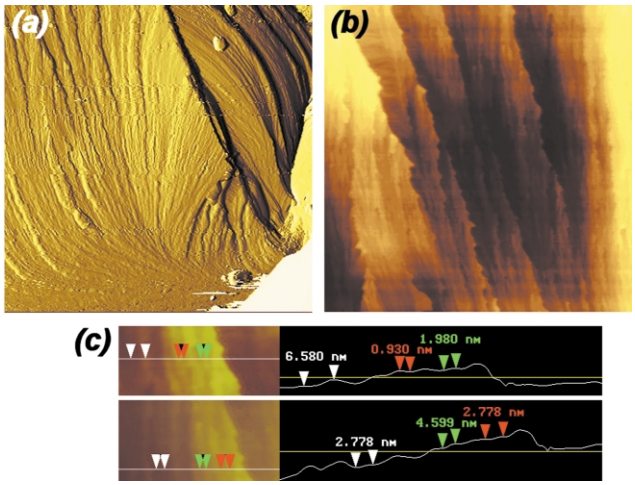

Fig. 3 AFM images of a {001} face: (a) 15 × 15 μm² amplitude image (b) 5 × 5 μm² height image. (c) cross-sectional analysis.

This work was supported by a grant from CONACYT Mexico and EPSRC advanced fellowship AF990985. The authors wish to thank N. Novak Tušar and A. Ristić for preparing the MnAPO-50 sample used in this study and Colin Cundy for very useful discussions.

Notes and references

1 O. Terasaki, T. Ohsuna, N. Ohnishi and K. Hiraga, *Curr. Opin. Sol. State Mater. Sci.*, 1997, **2**, 94–100.
2 S. Bazzana, S. Dumrul, J. Warzywoda, L. Hsiao, L. Klass, M. Knapp, J. A. Rains, E. M. Stein, M. J. Sullivan, C. M. West, J. Y. Woo, J. Sacco and Albert, *Stud. Surf. Sci. Catal.*, 2002, **142A**, 117–124.
3 S. Dumrul, S. Bazzana, J. Warzywoda, R. R. Biederman, J. Sacco and Albert, *Microporous Mesoporous Mater.*, 2002, **54**, 79–88.
4 G. Binnig, C. F. Quate and C. Gerber, *Phys. Rev. Lett.*, 1986, **56**, 930–933.
5 A. L. Weisenhorn, J. E. Macdougall, S. A. C. Gould, S. D. Cox, W. S. Wise, J. Massie, P. Maivald, V. B. Elings, G. D. Stucky and P. K. Hansma, *Science*, 1990, **247**, 1330–1333.
6 L. Scandella, N. Kruse and R. Prins, *Surf. Sci. Lett.*, 1993, **281**, 331–334; G. Binder, L. Scandella, A. Schumacher, N. Kruse and R. Prins, *Zeolites*, 1996, **16**, 2–6; S. Yamamoto, S. Sugiyama, O. Matsuoka, T. Honda, Y. Banno and H. Nozoye, *Microporous Mesoporous Mater.*, 1998, **21**, 1–6.
7 M. Komiyama and T. Yashima, *Jap. Journal Appl. Phys.*, 1994, **33**, 3761–3763.
8 S. Yamamoto, O. Matsuoka, S. Sugiyama, T. Honda, Y. Banno and H. Nozoye, *Chem. Phys. Lett.*, 1996, **260**, 208–214.
9 M. W. Anderson, J. R. Agger, J. T. Thornton and N. Forsyth, *Angew. Chem., Int. Ed. Engl.*, 1996, **35**, 1210–1213.
10 M. W. Anderson, J. R. Agger, N. Hanif, O. Terasaki and T. Ohsuna, *Sol. State Sci.*, 2001, **3**, 809–819.
11 S. Sugiyama, S. Yamamoto, O. Matsuoka, T. Honda, H. Nozoye, S. Qiu, J. Yu and O. Terasaki, *Surf. Sci.*, 1997, **377–379**, 140–144.
12 S. Sugiyama, M. Matsuoka and S. Yamamoto, *Microporous Mesoporous Mater.*, 2001, **48**, 103–110.
13 J. R. Agger, N. Pervaiz, A. K. Cheetham and M. W. Anderson, *J. Am. Chem. Soc.*, 1998, **120**, 10754–10759.
14 S. Sugiyama, S. Yamamoto, O. Matsuoka, H. Nozoye, J. Yu, G. Zhu, S. Qiu and O. Terasaki, *Microporous Mesoporous Mater.*, 1999, **28**, 1–7.
15 J. R. Agger, N. Hanif and M. W. Anderson, *Angew. Chem., Int. Ed. Engl.*, 2001, **20**, 4065–4067.
16 J. R. Agger, N. Hanif, C. S. Cundy, A. P. Wade, S. Dennison, P. A. Rawlinson and M. W. Anderson, *J. Am. Chem. Soc.*, 2003, **125**, 830–839.
17 R. Singh, J. Doolittle, M. A. George and P. K. Dutta, *Langmuir*, 2002, **18**, 8193–8197.
18 N. Novak Tušar , A. Ristić, A. Meden and V. Kaučič, *Microporous Mesoporous Mater.*, 2000, **37**, 303–311.
19 M. W. Anderson, N. Hanif, J. R. Agger, C.-Y. Chen and S. I. Zones, *Stud. Surf. Sci. Catal.*, 2001, **135**, 141.